Progress In Electromagnetics Research, Vol. 137, 727–740, 2013

FEATURES EXTRACTION OF ROTATIONALLY SYMMETRIC BALLISTIC TARGETS BASED ON MICRO-DOPPLER

Xiaoyi Pan[1, 2, *], Wei Wang[1], Jin Liu[2], Dejun Feng[2], Yongcai Liu[1], and Guoyu Wang[1, 2]

[1]School of Electronic Science and Engineering, National University of Defense Technology, Changsha 410073, China

[2]State Key Laboratory of Complex Electromagnetic Environment Effects on Electronics and Information System, Changsha 410073, China

Abstract—It is potentially useful to perform target identification using micro-Doppler features because they contain information on the geometrical structure of the target. In this paper, the m-D effect of the rotationally symmetric ballistic target (BT) is analyzed which reveals that the m-D is not a form of sinusoidal modulation due to the sliding-type scattering. Inspired by the extended Hough transform (EHT), a method to extract all the six parameters of the BT is proposed. The m-D effect and the performance of feature extraction algorithm are demonstrated by the measured data in a microwave anechoic chamber.

1. INTRODUCTION

When a radar transmits an electromagnetic wave to a target, the signal interacts with the target and returns back to the radar. In addition to the bulk motions, the target or any structure on the target may undergo micro-motion dynamics, such as the rotating rotor blades of a helicopter, the scanning antenna of a ship, the wheel of a ground vehicle and etc. [1–5]. The precession of the ballistic target (BT) is also a typical kind of micro-motion dynamics [6, 7]. Targets with micro-motion dynamics induce additional time-varying frequency modulation and generate sidebands about the Doppler frequency which is called micro-Doppler (m-D) effect [8]. Micro-Doppler is regarded as a unique signature of an object with movements where the uniqueness means

Received 1 February 2013, Accepted 6 March 2013, Scheduled 12 March 2013

* Corresponding author: Xiaoyi Pan (pan_xiao_yi@hotmail.com).

different micro-motions have dissimilar signatures. Micro-Doppler signatures might be extracted for radar target identification which is seen as a good method and a technique of great potential [6, 7, 9–17]. Since the m-D phenomenon is presented and researched by Chen et al., the extractions of the m-D signatures have developed rapidly [8, 18–22]. In the traditional works, the m-D effect induced by periodic rotation or vibration has been shown as a form of sinusoidal modulation in the spectrogram [21].

The Hough transform (HT) is treated as one of the most effective methods for the detection of straight lines, and the advantage of the HT is its stability and robustness when working on images where noise or discontinuity is present [23, 24]. In addition to the standard HT (SHT) that is used for detecting straight lines, the extended HT (EHT) can be used for detecting or extracting curves. Zhang et al. [25] apply the SHT and EHT in a spectrogram to detect the m-D signatures but its calculation cost increases with the dimension of parameters extremely [26]. In the precession of a ballistic target, due to the sliding-type scattering, the m-D effect is not a form of sinusoidal modulation and there are six parameters can be used in target identification included four m-D features and two structural parameters totally [27]. The cost burden of utilizing the EHT with six parameters is huge and the extracted features easily run into local optimums. Wang et al. [7] put forward a method to estimate the precession frequency and the precession angle, but not all the six features can be extracted by this method. Therefore, it is necessary to propose a method to extract the four precession features and two structural parameters simultaneously.

In this paper, all the six parameters of the rotational symmetric BT are extracted and calculated based on the m-D effect. In order to avoid the huge cost burden and local optimums, the three-parameter and four-parameter EHT are utilized instead of the EHT with six parameters. The remainder of this paper is outlined as follows. Section 2 models the m-D effect of the rotationally symmetric BT. Section 3 is dedicated to the feature extraction algorithm via the EHT in three steps. The m-D effect and extracted features of the BT model measured in a microwave anechoic chamber are presented in Section 4 which proves the validity of the proposed method. Finally, in Section 5, some conclusions are presented.

2. THE MODEL OF M-D FOR ROTATIONALLY SYMMETRIC BT

In this section, the m-D model of the rotationally symmetric BT is derived. The precession geometry for a rotationally symmetric BT

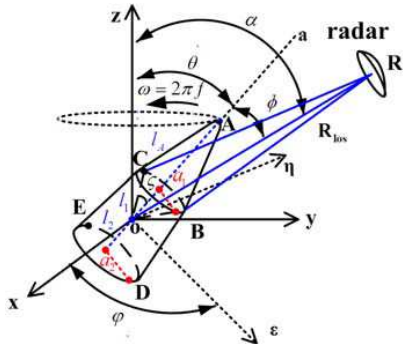

Figure 1. Geometry of radar and BT with precession.

is shown in Fig. 1. The radar coordinate system is defined by **oxyz** and the BT local coordinate system is defined by $\mathbf{o\varepsilon\eta z}$ with the same axis **oz** as the radar coordinate. The BT has precession along the axis **oz** with precession frequency f and spinning motion along the symmetric axis **oa** at the same time. For a rotationally symmetric target, spinning motion does not change the modulation effect and precession is only considered in the following analysis. The precession angle is assumed as θ and the distance between radar and the origin o is defined as $\|\mathbf{r}_{oR}\| = R_0$. Suppose that the radar light of sight (LOS) resides in the **yoz** plane, and the angle between LOS and the axis **oz** is denoted as α. The unit vector of the radar LOS can be expressed as $\mathbf{R}_{los} = [0, \sin\alpha, \cos\alpha]^T$ in **oxyz**.

The axis $\mathbf{o\varepsilon}$ is the projection of the axis **oa** onto the **oxyz** plane and the included angle is defined as φ. The corresponding initial rotation matrix and rotation matrix at time t are given by the following matrix solved by Euler's motion differential equations [21]

$$\Re_{init} = \begin{bmatrix} \cos\varphi_0 & -\sin\varphi_0 & 0 \\ \sin\varphi_0 & \cos\varphi_0 & 0 \\ 0 & 0 & 1 \end{bmatrix}, \quad \Re_t = \begin{bmatrix} \cos(2\pi ft) & -\sin(2\pi f) & 0 \\ \sin(2\pi ft) & \cos(2\pi f) & 0 \\ 0 & 0 & 1 \end{bmatrix} \quad (1)$$

where φ_0 is the initial angle of φ at $t = 0$, and $\varphi = \varphi_0 + 2\pi ft$.

The vertex of the cone is defined as A. Suppose that the upper and the lower circularity of the BT are located in the plane Π_2 and Π_3, respectively. Assume that the plane Π_1 decided by $\mathbf{R}_{los}$ and the axis **oa** intersects the plane Π_2 at the line Γ_1 and intersects the plane Π_3 at the line Γ_2. The line Γ_1 intersects the upper circularity of the BT at B and C and the line Γ_2 intersects the lower circularity at D and E. Theoretical computing and measuring experiments show that the backscattering of the BT is usually contributed by

the sliding-type scattering centers A, B, C, D and E as shown in Fig. 1 [7, 27]. The vectors of **oA**, **oB**, **oC**, **oD** and **oE** are defined as $\mathbf{r}_i\,(i = A, B, C, D, E)$ in **oxyz**. The radius of the upper and lower circularity is denoted as a_1 and a_2, respectively.

2.1. The m-D of the Scattering Center *A*

Then at time t the transient unit direction vector of the axis **oa** in the coordinate **oxyz** can be represented as

$$\begin{aligned}\mathbf{oa} &= \Re_t \cdot \Re_{init} \cdot [\sin\theta, 0, \cos\theta]^T \\ &= [\sin\theta\cos\varphi, \sin\theta\sin\varphi, \cos\theta]^T \end{aligned} \tag{2}$$

The angle between the axis **oa** and $\mathbf{R}_{los}$ is called as the aspect angle ϕ which satisfies that

$$\begin{aligned}\phi &= \cos^{-1}\left(\frac{\mathbf{oa}\cdot\mathbf{R}_{los}}{\|\mathbf{oa}\|\cdot\|\mathbf{R}_{los}\|}\right) \\ &= \cos^{-1}\left[\sin\alpha\sin\theta\sin\left(2\pi ft+\varphi_0\right)+\cos\alpha\cos\theta\right]\end{aligned} \tag{3}$$

where $\cdot$ is the dot product, and $\|\cdot\|$ represents the Euclidean norm. Thus, the micro-Doppler frequency of scattering center A due to the precession is

$$\begin{aligned}f_{mD-A} &= \frac{2}{\lambda}\frac{d}{dt}\left\|\mathbf{r}_A\right\|_{los} = \frac{2}{\lambda}\frac{d}{dt}\left[l_A\left(\mathbf{oa}\cdot\mathbf{R}_{los}\right)\right] \\ &= \frac{4\pi f l_A\sin\alpha\sin\theta}{\lambda}\cos\left(2\pi ft+\varphi_0\right)\end{aligned} \tag{4}$$

where l_A is the distance from o to A.

2.2. The m-D of the Scattering Center *B* or *C*

The normal vector of the plane Π_1 is defined as

$$\begin{aligned}\mathbf{n}_1 &= \mathbf{oa}\times\mathbf{R}_{los} \\ &= [\cos\alpha\sin\theta\sin\varphi-\sin\alpha\cos\theta, -\cos\alpha\sin\theta\cos\varphi, \sin\alpha\sin\theta\cos\varphi]^T\end{aligned} \tag{5}$$

where $\times$ denotes the cross product and the plane Π_1 is defined as

$$\mathbf{n}_1\cdot\mathbf{r}_{B,C} = 0 \tag{6}$$

Note that $\|\mathbf{n}_1\| = |\sqrt{1-(\cos\alpha\cos\theta+\sin\alpha\sin\theta\sin\varphi)^2}| = |\sin\phi|$ is not a unit vector.

The axis **oa** is perpendicular to Π_2, so the normal vector of Π_2 becomes

$$\mathbf{n}_2 = \mathbf{oa} = [\sin\theta\cos\varphi, \sin\theta\sin\varphi, \cos\theta]^T \tag{7}$$

and Π_2 is denoted as

$$\mathbf{n}_2 \cdot \mathbf{r}_{B,C} = l_1 \tag{8}$$

where l_1 is the distance from o to Π_2, and $\|\mathbf{n}_2\| = 1$ is an unit vector.

The vector $\mathbf{n}_1$ is perpendicular to the vector $\mathbf{n}_2$ and the direction of $\mathbf{r}_{B,C}$ is decided by $\mathbf{n}_1 \times \mathbf{n}_2$ which is represented as

$$\mathbf{n}_1 \times \mathbf{n}_2 = \begin{bmatrix} -\cos\alpha\sin\theta\cos\theta\cos\varphi - \sin\alpha\sin^2\theta\sin\varphi\cos\varphi \\ \sin\alpha - \cos\alpha\sin\theta\cos\theta\sin\varphi - \sin\alpha\sin^2\theta\sin^2\varphi \\ \cos\alpha\sin^2\theta\sin^2\varphi - \sin\alpha\sin\theta\cos\theta\sin\varphi + \cos\alpha\sin^2\theta\cos^2\varphi \end{bmatrix} \tag{9}$$

So the vector $\mathbf{r}_{B,C}$ can be derived as [27]

$$\mathbf{r}_{B,C} = k\left(\mathbf{n}_1 \times \mathbf{n}_2\right) + l_1 \cdot \mathbf{n}_2 \tag{10}$$

where $k = \pm a_1/|\sin\phi|$ is the rate of Γ_1 with "+" corresponding to $\mathbf{r}_B$ and "−" corresponding to $\mathbf{r}_C$. Then the length of the projection of $\mathbf{r}_{B,C}$ on the LOS is obtained as

$$\begin{aligned} \|\mathbf{r}_{B,C}\|_{los} &= \mathbf{r}_{B,C} \cdot \mathbf{R}_{los} = \left(k\left(\mathbf{n}_1 \times \mathbf{n}_2\right) + l_1 \cdot \mathbf{n}_2\right) \cdot \mathbf{R}_{los} \\ &= l_1\cos\phi \pm a_1\sin\phi \end{aligned} \tag{11}$$

Thus, the micro-Doppler frequency of scattering centre B or C due to the precession is given as

$$\begin{aligned} f_{mD-B,C} &= \frac{2}{\lambda}\frac{d}{dt}\|\mathbf{r}_{B,C}\|_{los} \\ &= \frac{4\pi f\sin\alpha\sin\theta}{\lambda}\cos\left(2\pi ft + \varphi_0\right) \\ &\quad \left[l_1 \pm a_1 \frac{\cos\alpha\cos\theta + \sin\alpha\sin\theta\sin\left(2\pi ft + \varphi_0\right)}{\sqrt{1-\left(\cos\alpha\cos\theta + \sin\alpha\sin\theta\sin\left(2\pi ft + \varphi_0\right)\right)^2}}\right] \end{aligned} \tag{12}$$

According to the similar method, $f_{mD-D,E}$ can also be computed as

$$\begin{aligned} f_{mD-D,E} &= \frac{4\pi f\sin\alpha\sin\theta}{\lambda}\cos\left(2\pi ft + \varphi_0\right) \\ &\quad \left[l_2 \pm a_2 \frac{\cos\alpha\cos\theta + \sin\alpha\sin\theta\sin\left(2\pi ft + \varphi_0\right)}{\sqrt{1-\left(\cos\alpha\cos\theta + \sin\alpha\sin\theta\sin\left(2\pi ft + \varphi_0\right)\right)^2}}\right] \end{aligned} \tag{13}$$

where l_2 is the distance from o to Π_3. It is evident from (12) and (13) that the m-D effect of the sliding-type scattering center B or C or D or E is not a form of sinusoidal modulation since that the second term changes along with time. Actually, the reason for this phenomenon is that the scattering centers slide on the surface of targets and its micro-motion is different from the target itself [27].

3. FEATURE EXTRACTION ALGORITHM VIA EHT

Since the micro-motion and structural information of the BT are contained by the curves on the m-D plane, the features can be extracted by detecting the parameters of these curves. The HT has been treated as one of the most popular and effective methods for the detection of line segments which was first introduced by Hough [28].

3.1. The EHT Algorithm

The HT maps the straight line on the image plane (x, y) into a point in the HT space via the following equation [25, 28]

$$\rho = x\cos\theta + y\sin\theta \tag{14}$$

where ρ is the length of the perpendicular through the origin o to the straight line and θ the included angle of the perpendicular and the x axis. All points (x_i, y_i) of the straight line in the image correspond to the point (ρ, θ) in the HT space just as depicted in Fig. 2. There are only two parameters of a straight line need to be extracted and so the HT of a straight line is a two-parameter transform which is also called SHT.

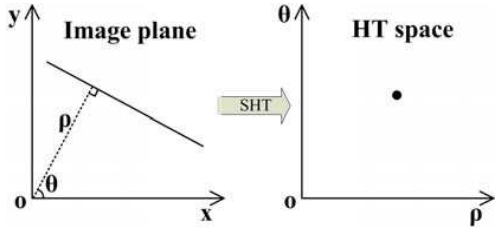

Figure 2. The sketch map of HT.

The HT has also been developed to extract curves of other shapes, such as sinusoid, circle and etc.. When there are more than two parameters of the curve, the EHT derived from the SHT is utilized. In general, the EHT can be used to extract the curves' features with the following basic principle: the curve is represented by the parameters $(a_1, a_2, \ldots, a_N)$, and each parameter accumulator counts the number of points (x_i, y_i) fitted into the curve equation [29]

$$g(a_1, a_2, \ldots, a_N, x_i, y_i) = 0 \tag{15}$$

The accumulator, which contains the local maxima in the EHT space, may imply the presence of a curve.

The m-D effects induced by the precession of the BT induce curves on the m-D plane. If the analytical expressions of the m-D curves are

obtained, the features of the BT can be extracted by constructing corresponding EHT transform equations. In the following, we use the EHT to discuss the m-D and structural features extraction algorithm.

3.2. Feature Extraction Algorithm

In this section, we present the feature extraction algorithm via the EHT in detail. The m-D effect of scattering centers *A, B, C, D* and *E* can be rewritten into a uniform form as

$$f_{mD-i}=\frac{4\pi f\sin\alpha\sin\theta}{\lambda}\cos\left(2\pi f+\varphi_0\right)\left(l_i+a_i\frac{\cos\phi}{\sqrt{1-\cos^2\phi}}\right),\quad i=A,B,C,D,E \tag{16}$$

where $l_B = l_C = l_1$, $l_D = l_E = l_2$, $a_A = 0$, $a_B = a_C = a_1$ and $a_D = a_E = a_2$ in a rotationally symmetric BT. The EHT can be used for detecting curves, and from (14) it can be seen that there are six parameters which are (f, α, θ, φ_0, l_i, a_i). The calculation cost of EHT with six parameters is huge and the extracted features easily run into local optimums. According to the characteristics of the precession, we first utilize the EHT with three parameters based on the m-D effect of the scattering centre *A*. After that the estimation of (f, φ_0) are obtained. Then we apply four-parameter EHT on the m-D of the scattering centers *B* (or *C* or *D* or *E*) to obtain the residual parameters. The concrete steps of the method are enumerated in the following list.

Step1 The m-D of the scattering center *A* scan be depicted as $f_{mD-A} = \eta_1\cos(2\pi ft+\varphi_0)$, where $\eta_1 = \frac{4\pi f}{\lambda}l_A\sin\alpha\sin\theta$. The following equation can be used to estimate the parameters on the m-D plane

$$\eta_1 = \frac{f_{mD-A}}{s\left(2\pi ft+\varphi_0\right)} \tag{17}$$

Equation (17) is readily expanded to define the mapping equation for the m-D plane (f_{mD-A}, t) to the three parameter space (η_1, f, φ_0). Applying the three-parameter EHT described in Equation (17) to the m-D plane and finding the maximum value of the EHT space, then the estimated parameter pairs ($\widehat{\eta}_1$, $\widehat{f}$, $\widehat{\varphi}_0$) can be obtained.

Step2 Taking ($\widehat{f}$, $\widehat{\varphi}_0$) from the step 1) as the known parameters, we can use the following equation to extract the residual parameters on the m-D plane

$$\eta_2 = \frac{f_{mD-i}-\eta_3\sin\theta\sin\alpha\cos\left(2\pi\widehat{f}t+\widehat{\varphi}_0\right)\frac{\sin\theta\sin\alpha\sin\left(2\pi\widehat{f}t+\widehat{\varphi}_0\right)+\cos\theta\cos\alpha}{\sqrt{1-\left[\sin\theta\sin\alpha\sin\left(2\pi\widehat{f}t+\widehat{\varphi}_0\right)+\cos\theta\cos\alpha\right]^2}}}{\sin\theta\sin\alpha\cos\left(2\pi\widehat{f}t+\widehat{\varphi}_0\right)} \tag{18}$$

where $\eta_2 = \frac{4\pi \widehat{f}}{\lambda} l_i$, $\eta_3 = \frac{4\pi \widehat{f}}{\lambda} a_i$, $i = B, C, D$ or E. Equation (18) is readily expanded to define the mapping equation for the m-D plane (f_{mD-i}, t) to the four parameter space $(\eta_2, \eta_3, \theta, \alpha)$. Applying the four-parameter EHT described in Equation (18) to the m-D plane to obtain the estimated parameter pairs $(\widehat{\eta}_2, \widehat{\eta}_3, \widehat{\theta}, \widehat{\alpha})$.

Step3 Then via a simple calculation, we have that $\widehat{l}_i = \frac{\widehat{\eta}_2 \lambda}{4\pi \widehat{f}}$, $\widehat{a}_i = \frac{\widehat{\eta}_3 \lambda}{4\pi \widehat{f}}$ and $\widehat{l}_A = \frac{\widehat{\eta}_1 \lambda}{4\pi \widehat{f} \sin \widehat{\alpha} \sin \widehat{\theta}}$.

Finally, the six parameters $(f, \alpha, \theta, \varphi_0, l_i, a_i)$ are all extracted after these three steps. The calculation cost is reduced and local optimums can also be avoided.

4. ANALYSES WITH MEASURED DATA

In this section, we show the m-D effect and the results of the proposed feature extraction algorithm based on the measured data. The measured data of a BT model is observed by a stepped-frequency (SF) waveform radar operating at 9.5 GHz in a microwave anechoic chamber as shown in Fig. 3(a). In each burst, a total of 201 stepped frequencies are used to cover a total of 1 GHz bandwidth which achieves 0.15 m range resolution. The pulse repetition frequency (PRF) of 67 Hz is used to cover the entire target. As shown in Fig. 3(b), the BT model with precession motion simulating system is designed which can simulate spinning motion and precession independently [27]. The BT model is similar to the one shown in Fig. 1 with $a_1 = a_2 = 0.2$ m, $l_1 = 0.7$ m, $l_2 = 0$ m and $l_A = 1.4$ m.

Taking three experiments for analysis, the precession parameters are listed in Table 1.

(a) (b)

Figure 3. Measurement of the BT model in the microwave anechoic chamber. (a) The measurement setting. (b) Precession model of BT.

Table 1. Parameters.

Experiments No.	θ (°)	α (°)	f (Hz)	φ_0 (°)
1	7.2	10.4	0.26	40
2	10	10.4	0.26	74
3	7.2	10.4	0.52	88

4.1. The m-D Effect of the Scattering Center A, B and C

Since the m-D effect of the BT with precession is time-varying, a joint time-frequency method is needed [17, 30]. Time-frequency methods include linear transforms, such as the short-time Fourier transform (STFT), and bilinear transforms, such as the Wigner-Ville distribution (WVD). In this section, the smoothed pseudo Wigner-Ville distribution (SPWVD) is utilized [31].

The m-D effect of the scattering centers A, B and C is show in Fig. 4 and Fig. 5. The white lines in each figure are the theoretical m-D results.

The m-D of the scattering center A is a form of sinusoidal modulation as shown in Fig. 4 while the m-D of the sliding-type scattering center B or C is not a form of sinusoidal modulation as shown in Fig. 5. The fluctuation of reflection characteristics

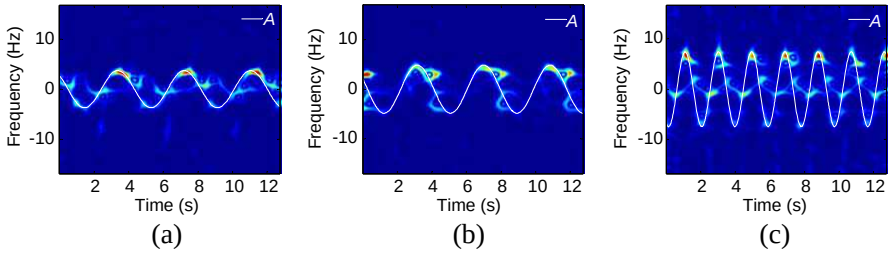

Figure 4. The m-D of the scattering center A. (a) Experiment 1. (b) Experiment 2. (c) Experiment 3.

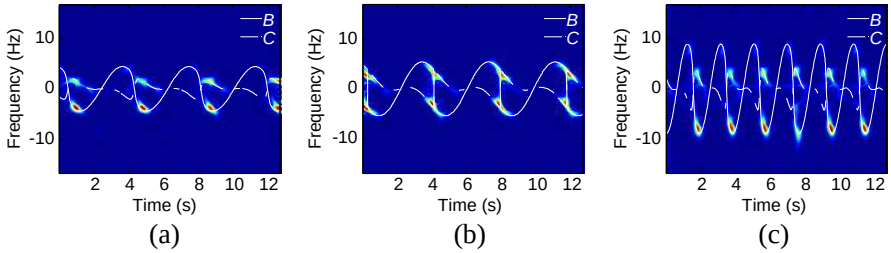

Figure 5. The m-D of the sliding-type scattering centers B and C. (a) Experiment 1. (b) Experiment 2. (c) Experiment 3.

with respect to the viewing angle change makes the m-D curves discontinuous but the periodical characteristics can still be seen from Fig. 4 and Fig. 5. The periodicity is corresponding to the precession frequency. Then applying the proposed algorithm on the m-D plane, the respective features can be extracted and calculated.

4.2. Extracted Results

Taking the experiment 1 for example, the EHT results of **step 1** and **step 2** are illustrated in Fig. 6(a) and Fig. 6(b), respectively. From

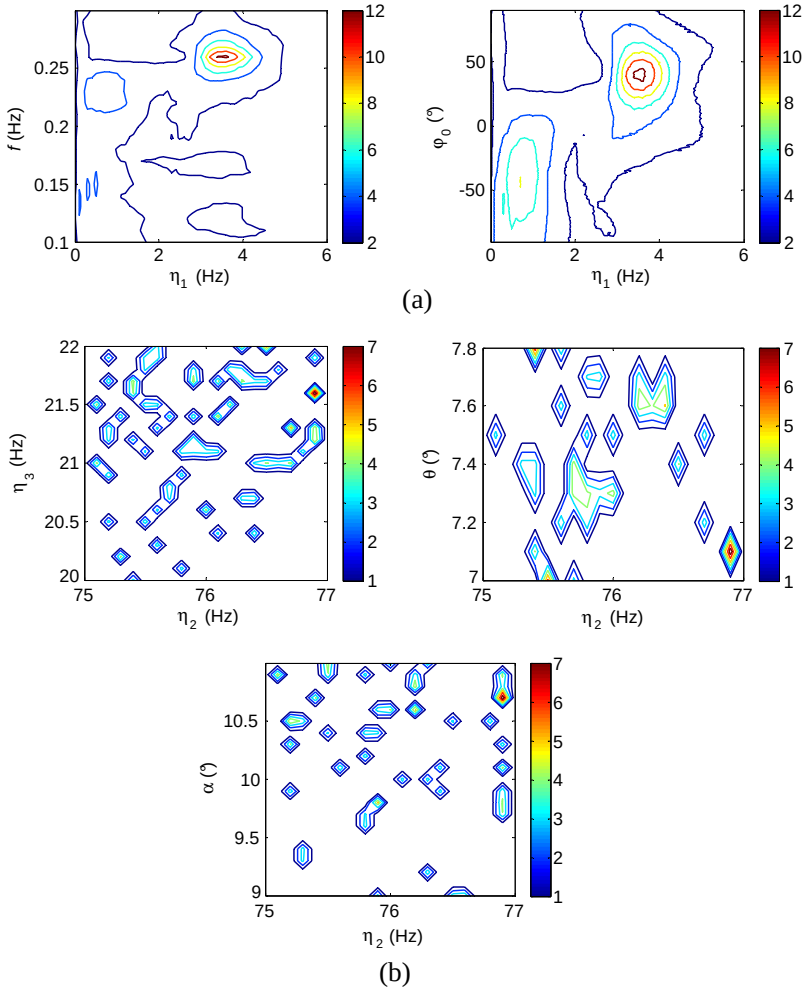

Figure 6. The EHT results of experiment 1. (a) The three-parameter EHT results of Step1. (b) The four-parameter EHT results of Step2.

Fig. 6(a), we can obtained that $\widehat{\eta}_1 = 3.6\,\text{Hz}$, $f = 0.26\,\text{Hz}$, $\varphi_0 = 39°$ and from Fig. 6(b) $\widehat{\eta}_2 = 76.9\,\text{Hz}$, $\widehat{\eta}_3 = 21.6\,\text{Hz}$, $\theta = 7.1°$ and $\alpha = 10.6°$ are extracted by choosing the maximum value of each figure. Then the residual parameters can be calculated as $\widehat{l}_1 = 0.706\,\text{m}$, $\widehat{a}_1 = 0.198\,\text{m}$ and $\widehat{l}_A = 1.440\,\text{m}$.

Similarly, applying the proposed algorithm on all the three experiments, respective parameters are obtained and revealed in Table 2.

Table 2. Results of extracted features.

Experiment No.	$\widehat{\theta}$ (°)	$\widehat{\alpha}$ (°)	$\widehat{f}$ (Hz)	φ_0 (°)	$\widehat{l}_i$ (m), $i = A, 1, 2$	$\widehat{a}_i$ (m), $i = 1, 2$
1	7.1	10.6	0.26	39.0	1.440,0.706,0.005	0.198,0.196
2	9.5	10.2	0.26	75.0	1.442,0.695,0.003	0.198,0.197
3	7.5	10.7	0.54	90	1.451,0.694,0.003	0.195,0.199

Compared the extracted results with the real structural parameters and precession features mentioned in 4.1, the extracted results are in accordance with the real features.

5. CONCLUSIONS

The m-D effect of the rotationally symmetric BT is modeled and analyzed in this paper. The theoretical analysis and experiments indicate that the m-D effect of the sliding-type scattering centers on the BT is not a form of sinusoidal modulation. The reason is that the scattering centers slide on the surface of targets and its micro-motion is different from the target itself. The four precession parameters and the two structural features are extracted and calculated in three steps. The m-D effect and the performance of the proposed feature extraction algorithm are verified by the analysis based on the measured data in a microwave anechoic chamber.

REFERENCES

1. Park, J.-H., H. Lim, and N.-H. Myung, "Modified Hilbert-Huang transform and its application to measured micro Doppler signatures from realistic jet engine models," *Progress In Electromagnetics Research*, Vol. 126, 255–268, 2012.
2. Felguera-Martìn, D., T. González-Partida, and M. Burgos-García, "Interferometric ISAR imaging on maritime target applications:

Simulation of realistic targets and dynamics," *Progress In Electromagnetics Research*, Vol. 132, 571–586, 2012.

3. Bai, X., F. Zhou, M. Xing, and Z. Bao, "High resolution ISAR imaging of targets with rotating parts," *IEEE Transactions on Aerospace and Electronic Systems*, Vol. 47, No. 4, 2530–2543, 2011.
4. Liu, B. and W. Chang, "Range alignment and motion compensation for missile-borne frequency stepped chirp radar," *Progress In Electromagnetics Research*, Vol. 136, 523–542, 2013.
5. Pan, X., W. Wang, D. Feng, J. Huang, Q. Fu, and G. Wang, "Rotational micro-motion modulated jamming for countering ISAR based on intermittent sampling repeater," *Progress In Electromagnetics Research C*, Vol. 36, 41–56, 2013.
6. Gao, H., L. Xie, S. Wen, and Y. Kuang, "Micro-Doppler signature extraction from ballistic target with micro-motions," *IEEE Transactions on Aerospace and Electronic Systems*, Vol. 46, No. 4, 1969–1982, 2010.
7. Wang, T., X. Wang, Y. Chang, J. Liu, and S. Xiao, "Estimation of precession parameters and generation of ISAR images of ballistic missile targets," *IEEE Transactions on Aerospace and Electronic Systems*, Vol. 46, No. 4, 1983–1995, 2010.
8. Chen, V. C., "Analysis of radar micro-Doppler signature with time-frequency transform," *Proceedings of the IEEE Workshop on Statistical Signal and Array Processing (SSAP)*, 463–466, Pocono, PA, 2000.
9. Li, H. J. and K. M. Li, "Application of wavelet transform in target identification," *Progress In Electromagnetics Research*, Vol. 12, 57–73, 1996.
10. Han, S.-K., H.-T. Kim, S.-H. Park, and K.-T. Kim, "Efficient radar target recognition using a combination of range profile and time-frequency analysis," *Progress In Electromagnetics Research*, Vol. 108, 131–140, 2010.
11. Guo, K. Y., Q. Li, and X. Q. Sheng, "A precise recognition method of missile warhead and decoy in multi-target scene," *Journal of Electromagnetic Waves and Applications*, Vol. 24, No. 5, 641–652, 2010.
12. Park, J.-I. and K.-T. Kim, "A comparative study on ISAR imaging algorithms for radar target identification," *Progress In Electromagnetics Research*, Vol. 108, 155–175, 2010.
13. Zubair, M., M. J. Mughal, and Q. A. Naqvi, "An exact solution of the cylindrical wave equation for electromagnetic field

in fractional dimensional space," *Progress In Electromagnetics Research*, Vol. 114, 443–455, 2011.

14. Kurrant, D. and E. Fear, "Extraction of internal spatial features of inhomogeneous dielectric objects using near-field reflection data," *Progress In Electromagnetics Research*, Vol. 122, 197–221, 2012.
15. Park, S. H., J. H. Lee, and K. T. Kim, "Performance analysis of the scenario-based construction method for real target ISAR recognition," *Progress In Electromagnetics Research*, Vol. 128, 137–151, 2012.
16. Yang, W., Y. Liu, G.-S. Xia, and X. Xu, "Statistical mid-level features for building-up area extraction from high-resolution polarimetric SAR imagery," *Progress In Electromagnetics Research*, Vol. 132, 233–254, 2012.
17. Wang, Y., Q. Song, T. Jin, Y. Shi, and X. Huang, "Sparse time-frequency representation based feature extraction method for landmine discrimination," *Progress In Electromagnetics Research*, Vol. 133, 459–475, 2013.
18. Chen, V. C., R. Lipps, and M. Bottoms, "Advanced synthetic aperture radar imaging and feature analysis," *Proceedings of International Conference on Radar*, 22–29, 2003.
19. Chen, V. C., F. Li, S. S. Ho, and H. Wechsler, "Analysis of micro-Doppler signatures," *IEE Proc. — Radar Sonar Navig.*, Vol. 150, No. 4, 271–276, 2003.
20. Chen, V. C., "Spatial and temporal independent component analysis of micro-Doppler features," *Proceedings of International Conference on Radar*, 348–353, 2005.
21. Chen, V. C., F. Li, S. Ho, and H. Wechsler, "Micro-Doppler effect in radar-phenomenon, model, and simulation study," *IEEE Transactions on Aerospace and Electronic Systems*, Vol. 24, No. 24, 1–21, 2006.
22. Chen, V., *The Micro-Doppler Effect in Radar,* Artech House Radar Library, 2011.
23. Barbarossa, S., "Analysis of multicomponent LFM signals by a combined Wigner-Hough transform," *IEEE Transactions on Signal Processing*, Vol. 43, No. 6, 1511–1515, 1995.
24. Xue, W. and X. W. Sun, "Multiple targets detection method based on binary Hough transform and adaptive time-frequency filtering," *Progress In Electromagnetics Research*, Vol. 74, 309–317, 2007.
25. Zhang, Q., T. S. Yeo, H. S. Tan, and Y. Luo, "Imaging of a moving target with rotating parts based on the Hough transform," *IEEE*

Transactions on Geoscience and Remote Sensing, Vol. 46, No. 1, 291–299, 2008.

26. Li, K., X. Liang, Q. Zhang, Y. Luo, and H. Li, "Micro-Doppler signature extraction and ISAR imaging for target with micromotion dynamics," *IEEE Geoscience and Remote Sensing Letters*, Vol. 8, No. 3, 411–415, 2011.
27. Ma, L., J. Liu, T. Wang, Y. Li, and X. Wang, "The micro-Doppler character of sliding-type scattering center on rotationally symmetric target," *Science in China Series F: Information Science*, Vol. 53, No. 1, 1–18, 2010.
28. Hough, P. V. C., "Methods and means for recognizing complex patterns," US Patent 3069654, 1962.
29. Luo, Y., Q. Zhang, C. Qiu, X. Liang, and K. Li, "Micro-Doppler effect analysis and feature extraction in ISAR imaging with stepped-frequency chirp signals," *IEEE Transactions on Geoscience and Remote Sensing*, Vol. 48, No. 4, 2087–2098, 2010.
30. Han, S.-K., H.-T. Kim, S.-H. Park, and K.-T. Kim, "Efficient radar target recognition using a combination of range profile and time-frequency analysis," *Progress In Electromagnetics Research*, Vol.108, 131–140, 2010.
31. Wu, Y. and D. C. Munson, Jr., "Wide-angle ISAR passive imaging using smoothed pseudo Wigner-Ville distribution," *Proceedings of the 2001 IEEE radar Conference*, 363–368, 2001.